2.2 Reference Characterization of the Advanced ODS 14YWT-SM12 Heat Used in HFIR JP30/31 Neutron Irradiation Experiment — D. T. Hoelzer, K. A. Unocic, E. T. Manneschmidt and M. A. Sokolov (Oak Ridge National Laboratory)

OBJECTIVE

Obtain results from characterization of the microstructures and mechanical properties of specimens produced from three heats of the advanced oxide dispersion strengthened (ODS) 14YWT-SM12 ferritic alloys with different extrusion temperatures to compare with irradiated specimens from the HFIR JP30/31 neutron irradiation experiment.

SUMMARY

Plate samples of ODS 14YWT-SM12 were produced from material extruded at 850, 1000 or 1150ºC followed by rolling parallel to the extrusion direction at 1000ºC to 50% reduction in thickness. Results from tensile tests conducted at 25ºC to 800ºC showed slightly lower strengths, but significantly better ductility in all the 14YWT-SM12 heats compared to results from previous 14YWT heats. The microstructural characteristics observed by SEM and TEM analyses showed that slightly larger grains with less uniformity in grain size had formed in the SM12 heats compared to previous 14YWT heats. The observed differences in the mechanical properties and grain structures of the SM12 heats compared to previous 14YWT heats were most likely due to the lower O, C and N levels achieved in producing the 14YWT-SM12 heats.

PROGRESS AND STATUS

Introduction

The advanced oxide dispersion strengthened (ODS) 14YWT ferritic alloy was developed for extreme neutron irradiation environments such as those encountered in plasma facing components of fusion reactors. The primary goal in development of the ODS 14YWT ferritic alloy was to obtain ultra-fine grains plus a high concentration of nano-size oxide particles, or Y-, Ti- and O-enriched nanoclusters (NC), that are responsible for the excellent strength and creep properties at elevated temperatures and good fracture toughness properties at low temperatures. In addition, the very high interfacial area associated with the ultra-fine grain structure and high concentration of NC provides high sink strength for trapping point defects that make 14YWT a very promising material for achieving high tolerance to neutron irradiation damage. However, there have only been a few studies conducted on 14YWT that consisted of neutron irradiations to relatively high doses. To date, SS-J3, DCT and TEM specimens from past 14YWT heats have only been included in two MATRIX collaborations that were conducted in the past between DOE (LANL)/ CEA, Saclay using the Phenix Reactor.

In 2011, the US Fusion Materials Program in collaboration with JAEA sponsored the construction of the JP30/31 neutron irradiation experiment at HFIR. This experiment was planned to irradiate specimens from several ferritic alloys in 3 sub-capsules at temperatures of 300ºC, 400ºC and 650ºC to a neutron dose of ~20 to 25 dpa depending on the final number of cycles. The specimen matrix included a variety of test specimens that were fabricated from the ODS 14YWT-SM12 ferritic alloy [1]. This alloy was developed in the NE Fuel Cycle Research and Development (FCRD) program and was produced by mechanical alloying to form three

heats differentiated by extruding the ball-milled powder at 1150ºC (SM12a), 1000ºC (SM12c) and 850ºC (SM12d). Plates were fabricated from the extruded bars by rolling either parallel or normal (cross) to the extrusion axis. The specimens fabricated from the plates consisted of SS-J3, APFIM, TEM, DCT, M5PCCVN and MMPC to provide for detailed PIE studies of the microstructure and mechanical properties in the future. The purpose of this report is to cover the preliminary results obtained from the reference characterization of the microstructures and mechanical properties of the 14YWT-SM12 heats to compare with irradiated specimens from the HFIR JP30/31 experiment.

Processing of 14YWT-SM12

The 14YWT-SM12 heat was produced by mechanical alloying (MA) using gas-atomized powder produced by Special Metals with nominal composition of Fe-14Cr-3W-0.4Ti (Fe pre-alloyed) and nano-size (17-31 nm) Y_2O_3 powder produced by Nanophase, Inc. The blended powder consisting of 99.7% Fe pre-alloyed and 0.3% Y_2O_3 powder (wt. %) was ball milled using the Zoz Simoloyer CM08 high kinetic energy mill for 40 h in an Ar atmosphere. Three 750 g batches of ball-milled powder were sealed in 2.9 inch diameter mild steel cans and degassed at 400ºC in vacuum before being hermetically sealed. The three sealed cans were annealed for 1 h at 850ºC and then 1 h at 1150ºC (SM12a heat), 1000ºC (SM12c heat) and 850ºC (SM12d heat) followed by extrusion. The cans were extruded through a rectangular shaped die to form bars. The extruded bars were annealed at 1000ºC for 1 h in vacuum and then cut into 3 sections of equal lengths for rolling. One section of each heat was rolled parallel (PR) to the extrusion direction at 1000ºC to ~50% reduction in thickness to form plates.

Chemical analysis was performed on ball milled powder and an extruded sample to correlate the interstitial O, C and N levels with processing of the ODS 14YWT-SM12 ferritic alloy. The results of the chemical analysis are shown in Table 1. The O and C levels were very similar between the ball milled powder and extruded sample. However, the results showed a very low N level in the ball-milled powder that increased significantly after extrusion. The reason for this increase is not apparent. Typically, poor ball milling conditions lead to significant contamination of both O and N due to the ingress of air into the chamber during ball milling. However, the O level was controlled very well using the ball milling conditions for the 14YWT-SM12 powder. Contamination of the ball-milled powder during degassing is not likely since the powder was degassed at 400ºC in vacuum. After degassing, the can was then sealed by crimping the tube connecting the can to the vacuum pump. Thus, to help understand the reason for the high N level after extrusion, a second sample will be prepared from 14YWT-SM12 and sent to DIRATS for independent chemical analysis.

Table 1. Comparison of the O, C and N levels of the ball milled powder and bulk extruded sample of 14YWT-SM12.

Condition	Composition (wppm)		
	O	C	N
Ball milled powder	1184	128	117
Extruded sample	1080	150	1740

Preparation of Specimens

Specimens were fabricated from plates of the three 14YWT-SM12 heats that were rolled parallel to the extrusion direction. The fabricated specimens consisted of miniature tensile (SSJ3; 5 x 1.4 x 0.75 mm gage), disk compact tension fracture toughness (DCT; ~Ø12.5 x 0.2 mm), TEM disk (Ø3 x 0.25 mm) and small angle neutron scattering coupon (SANS; 10.2 x 10.2 x 2.5 mm). The list showing the type, orientation and number of specimens prepared for the reference characterization studies is shown in Table 2. The DCT specimens were fabricated with the test load oriented parallel, or longitudinal (L), and the notch for pre-cracking oriented normal, or transverse (T), to the extrusion direction of the plates. Similarly, the SS-J3 tensile specimens were fabricated with the gage section lying parallel (L) or transverse (T) to the extrusion direction of the plates.

Table 2. Specimens fabricated from the plates of the three 14YWT-SM12 heats for the reference characterization studies.

Plate heat	Specimen Type	Orientation	Number
SM12a	DCT	L-T	13
	SS-J3	L	12
	SS-J3	T	5
	SANS	-	2
	TEM	-	3
SM12c	DCT	L-T	12
	SS-J3	L	19
	SS-J3	T	6
	SANS	-	2
	TEM	-	2
SM12d	DCT	L-T	16
	SS-J3	L	15
	SS-J3	T	12
	SANS	-	2
	TEM	-	1

Characterization Study

The purpose of the reference characterization study was to correlate the different processing conditions for producing the three 14YWT-SM12 heats with their microstructures and mechanical properties. The study focuses on microstructure analysis using SEM, TEM and possibly Atom Probe and on mechanical properties using hardness, tensile and fracture toughness tests. The results from this study will be compared later to those obtained from PIE of the irradiated specimens from JP30/31. The results of this comparison will help guide future development of the ODS 14YWT ferritic alloy for advanced nuclear energy systems including plasma facing components of fusion reactors.

Microstructural Analysis

The microstructures of the three 14YWT-SM12 heats were investigated using Transmission Electron Microscopy (TEM). The initial investigation was performed on electro-polished thin foil disk specimens that were prepared from each heat. The thin foil specimens were examined using the Philips CM200 FEG-TEM/STEM (Field Emission Gun-TEM/Scanning Transmission Electron Microscope) with XEDS, EELS/EFTEM (X-ray Energy Dispersive Spectroscopy, Electron Energy Loss Spectroscopy/Energy-Filtered TEM). The analysis of the grain structure was conducted using bright-field (BF) diffraction contrast imaging. Energy-Filtered TEM was used to investigate the oxide particles that formed in the 14YWT-SM12a heat. This heat was investigated first since the higher extrusion temperature (1150ºC) used to produce it most likely resulted in the largest oxide particle size compared to the oxide particles that formed in the two heats extruded at lower temperatures.

The microstructural characteristics of the three 14YWT-SM12 heats observed by BF imaging at low magnifications are shown in Figure 1. The analysis showed that all three heats contained grains that were similar in size, size distribution and morphology. The microstructures consisted of grains that were mostly less than 1 mm in size and wide distribution of sizes. The grains were slightly elongated in the extrusion and rolling directions. These results were consistent with those obtained from SEM analysis [1]. In addition, the dislocation analysis showed a relatively low dislocation density in the grains of the three heats.

The salient microstructural features of 14YWT-SM12 observed by BF imaging at high magnifications are shown in Figures 2, 3 and 4 for the SM12a, SM12c and SM12d heats, respectively. The results showed that the in matrix regions of the grains were mostly featureless. However, a low number density of visible particles larger than ~10 nm was observed in all the heats, but that these particles were non-uniformly distributed. Some of the grains in the heats showed the presence of a high density of very small particles. For example, the particles observed with dark contrast in the BF micrographs for the SM12d heat in Figure 4 were <4 nm in size. These small particles are most likely the Ti-, Y- and O-enriched nanoclusters, but this inference will need to be confirmed by EFTEM and atom probe in the future.

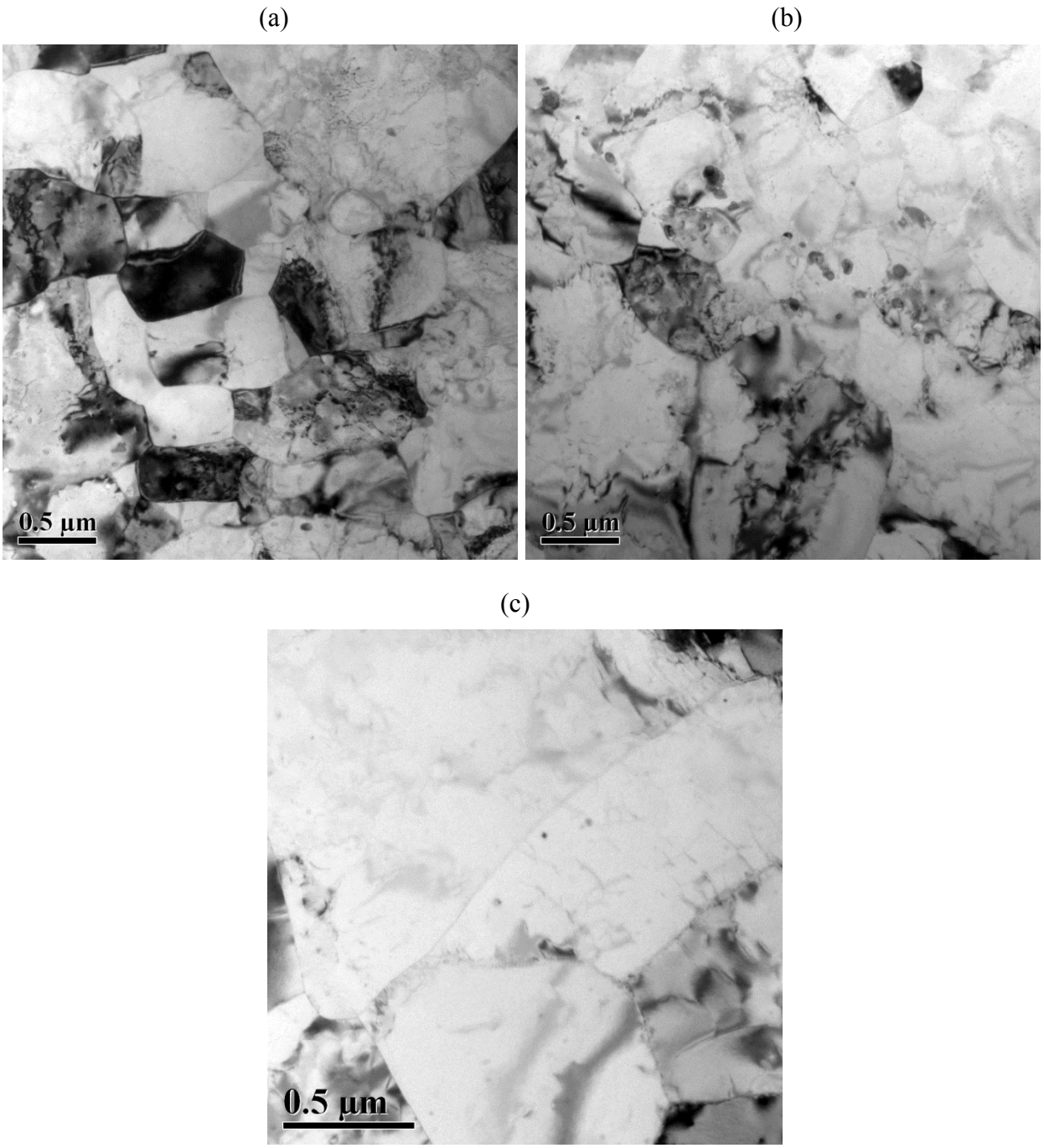

Figure 1. TEM BF micrographs showing the general microstructural characteristics of the (a) 14YWT-SM12a, (b) 14YWT-SM12c and (c) 14YWT-SM12d heats.

The results of the EFTEM analysis of the oxide particles that formed in the 14YWT-SM12a heat are shown in Figure 5. Several particles appearing with dark contrast near the edge of the thin foil specimen are observed in the Fe-M jump ratio map shown in Figure 5a. The dark contrast results from local displacement of Fe atoms by the particle that lowers the inelastic scattering

intensity in that region. There was one large particle that was ~50 nm in diameter and several particles <10 nm in size that were observed in the Fe M-jump ratio map. These particles along with several additional particles <10 nm in size are observed in the Ti L-composition map shown in Figure 5b. The bright contrast indicated that Ti atoms are associated with these particles, which is consistent with the small particles being Ti-, Y- and O-enriched nanoclusters.

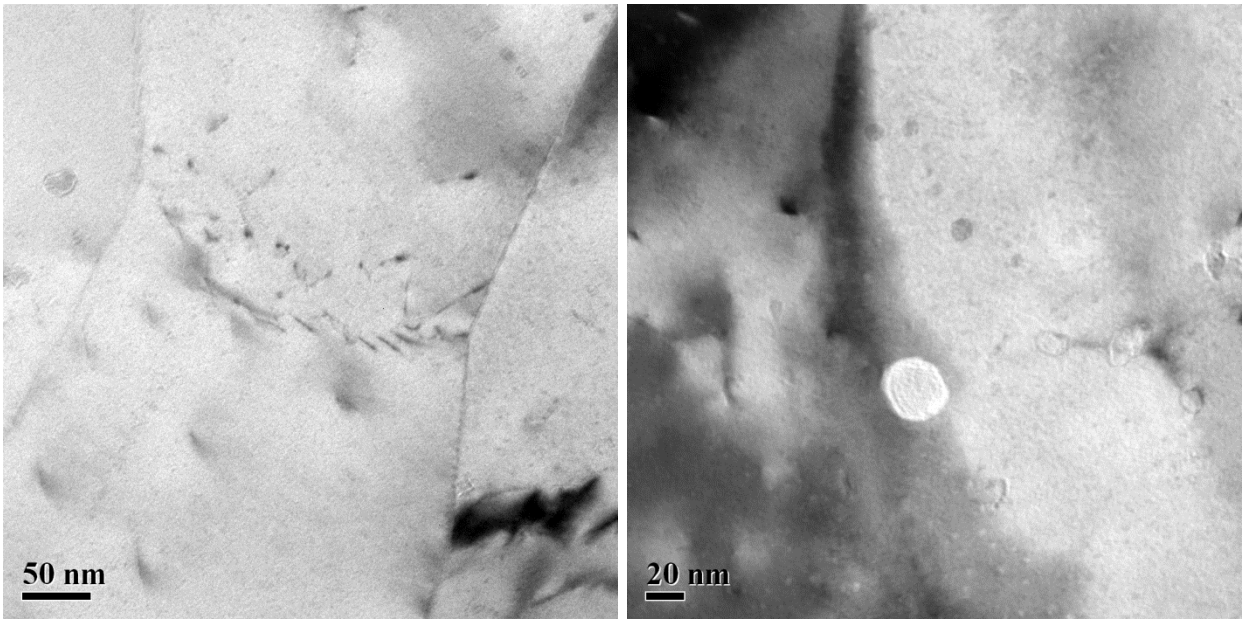

Figure 2. High magnification TEM BF micrographs showing the in-matrix regions of grains in the 14YWT-SM12a heat.

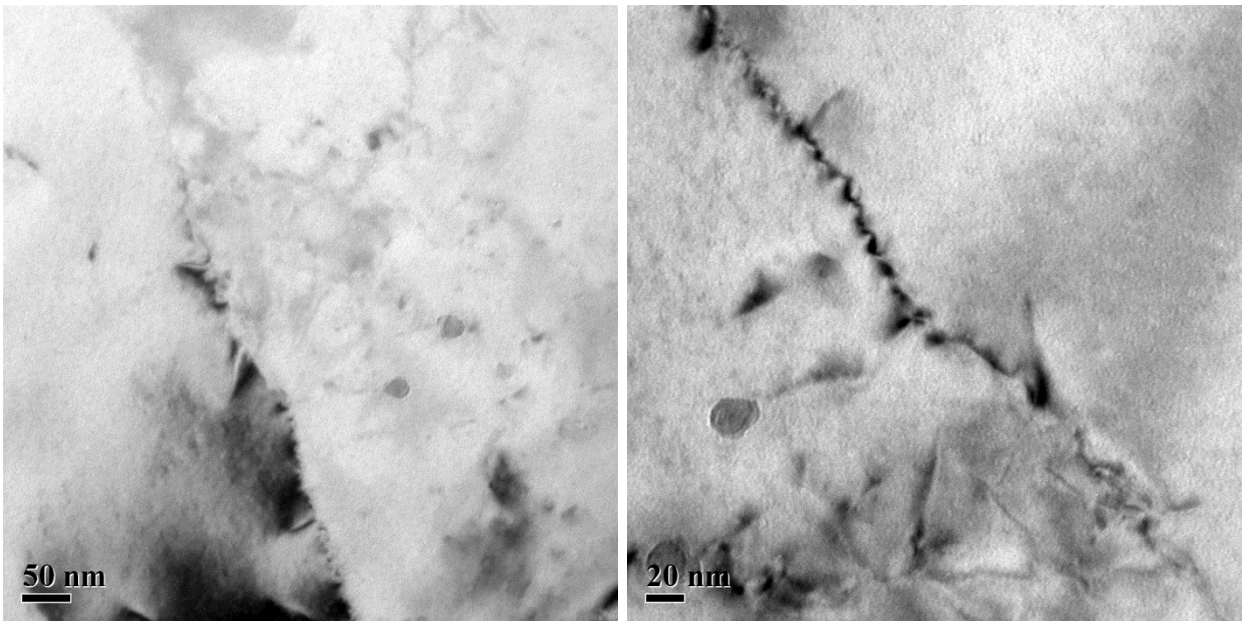

Figure 3. High magnification TEM BF micrographs showing the in-matrix regions of grains in the 14YWT-SM12c heat.

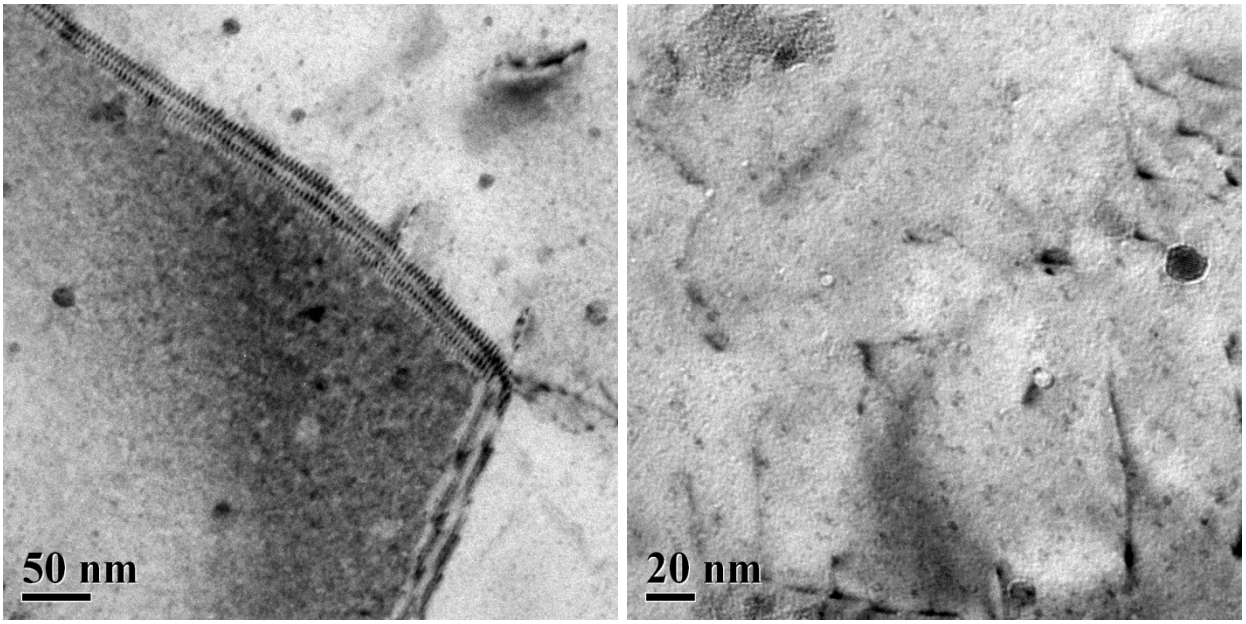

Figure 4. High magnification TEM BF micrographs showing the in-matrix regions of grains in the 14YWT-SM12d heat.

The EFTEM results were surprising since past research has shown that the Fe-M jump ratio method was very effective for producing reliable maps showing the size and distribution of oxide particles with resolution approaching 1 nm [2]. The Ti L-jump ratio and L-composition maps obtained from the same regions were typically noisier with lower resolution. However, the EFTEM results of this study showed that the Ti L-composition map resulted in better resolution for observing small particles. There may be several reasons for these differences in results. Results from the past investigations were obtained with the Philips CM30 TEM, which was a 300 kv instrument with a LaB_6 filament that produced a high probe current that achieved high-resolution EFTEM maps. The results for 14YWT-SM12a were obtained with the Philips CM200 FEG-TEM/STEM, which is a 200 kv instrument with an Schottky field emission gun that does not produce as high a probe current. The resolution of EFTEM maps is related to the incident electron energy and to signal-to-noise issues, which partly explains why EFTEM maps obtained from the CM30 showed better resolutions than those from the CM200. Another factor was that the Fe M post-edge and pre-edge maps used for producing the Fe M-jump ratio map showed low inelastic scattering intensity that contributed to poor signal-to-noise ratio. Also, the t/l image shown in Figure 5c indicated that the thin foil region was very thin. The t/l is obtained from:

$$t/l = \ln(\text{unfiltered image}/\text{zero-loss image})$$

where l is the inelastic scattering mean free path and is ~140 nm for the 14YWT composition. The diagonal line shown in Figure 5c is plotted in Figure 5d to show the variations in t/l with distance. The results indicated that most of the thin foil region where the EFTEM analysis was performed on had a thickness that was <30 nm. This resulted in low signal. Thus, the lower accelerating voltage and probe current of the CM200 and the thin thickness of the thin foil region contributed to the poor resolution of the Fe M-jump ratio map. Evidently, the method

used for removing the background near the Ti L ionization edge to calculate the Ti L-composition map was not as sensitive to the low signal-to-noise.

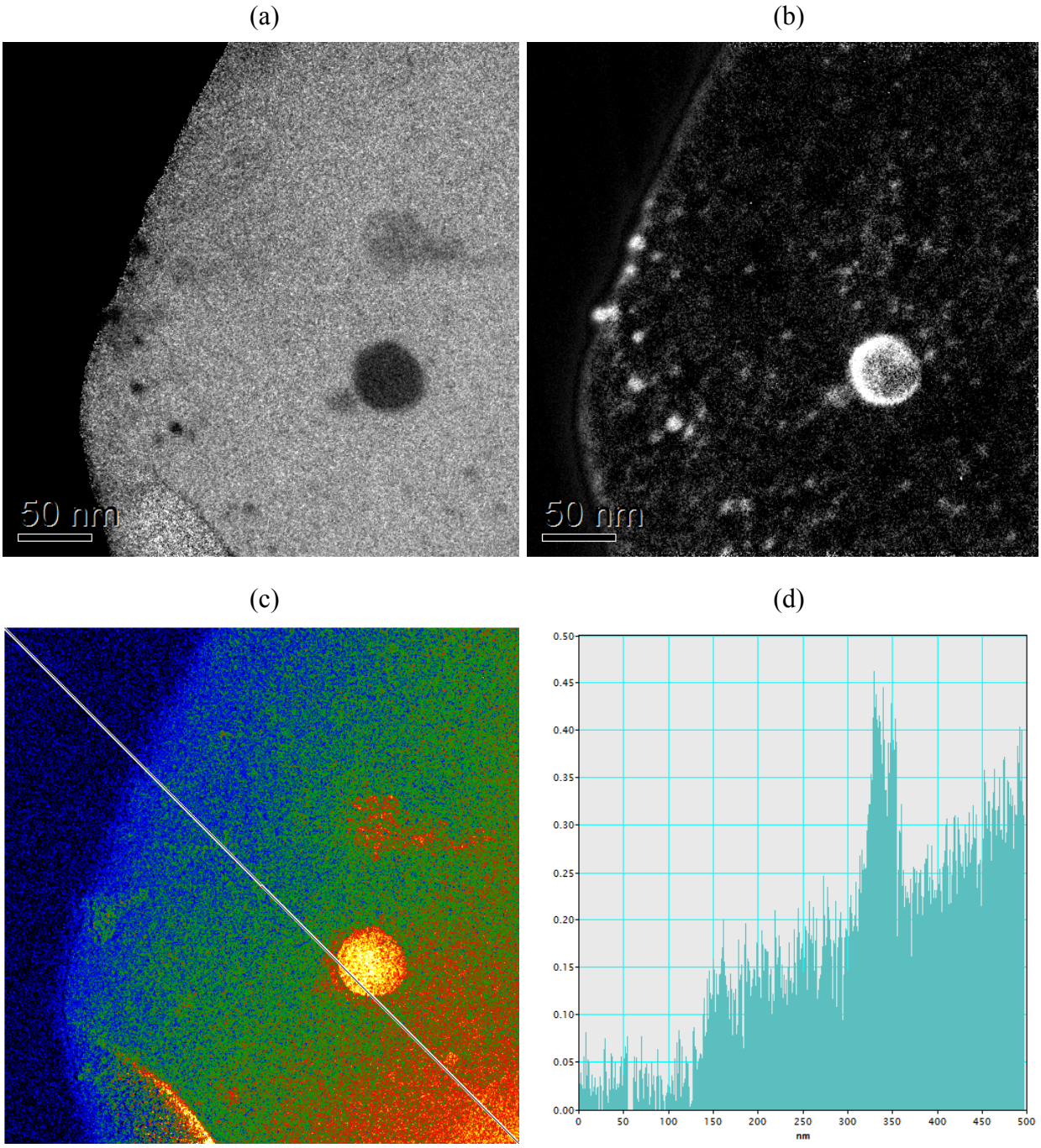

Figure 5. EFTEM analysis of 14YWT-SM12a near the thin foil edge showing (a) Fe M-jump ratio map, (b) Ti L composition map, (c) t/l thickness map and (d) thickness profile associated with line observed in the thickness map in (c).

Tensile Properties Analysis

Tensile tests were performed on SS-J3 specimens of the 14YWT-SM12 heats over the temperature range from room temperature (25ºC) to 800ºC using a strain rate of 1 x 10^{-3} s^{-1}. The results of the tensile tests are shown in Figure 6. The results indicated that values for the yield and ultimate tensile stresses and uniform and total elongations of the three heats were very similar over the temperature range. Compared to tensile properties of previous 14YWT heats, the 14YWT-SM12 heats showed generally lower strength and higher ductility properties. The yield stresses and ultimate tensile strengths of the SM12 heats were all near ~1050 MPa and ~1200 MPa, respectively, at room temperature and decreased with temperature to ~260 MPa and ~300 MPa, respectively, at 800ºC. The uniform and total elongations of the SM12 heats were ~9-10% and ~21-24%, respectively, at room temperature, which is significantly better than the 1 to 2% uniform elongation typically observed in previous 14YWT heats. The changes in uniform and total elongations with increasing temperatures showed similar trends for the SM12a and SM12c heats compared to the SM12d heat. For the SM12a and SM12c heats, the uniform elongation decreased slightly with temperatures while the total elongation remained nearly constant up to 400-500ºC and then increased to a peak value near 700ºC. The changes in uniform and total elongations with increasing temperatures were much less for the SM12d heat.

The comparison of stress-strain curves for the 14YWY-SM12 heats at room temperature is shown in Figure 7. The stress-strain curves of the three SM12 heats are remarkably similar. The stress increases to the yield point and then increases with strain to similar values of ultimate tensile strengths of ~1150-1200 MPa and uniform strains of ~9%. After plastic instability denoted by necking of the specimens, the deformation proceeded with decreasing stress with increasing strain until failure, which occurred at similar fracture stresses and total elongations.

The sets of stress-strain curves that have currently been obtained from tensile tests over the temperature range from 25ºC to 800ºC are shown in Figures 8, 9 and 10 for the SM12a, SM12c and SM12d heats, respectively. The analysis of the curves showed that gradual work hardening occurred in the specimens tested at temperatures up to 400ºC that resulted in higher values of uniform strain. Above 400ºC, the work hardening saturates quickly resulting in lower values of uniform strain. However, the stress tends to decrease very slowly with increasing strain, indicating that deformation may be following a pseudo-creep mechanism that is enhanced by the relatively small grain size of the SM12 heats. In most cases, this deformation behavior covers more than 10% strain before the stress begins to decrease more rapidly with increasing strain leading to ultimate failure of the specimen.

The results obtained from the reference characterization studies to date have revealed several interesting aspects of the effect that different processing conditions had on the microstructures and tensile properties of the three 14YWT-SM12 heats. One point is that the relatively lower strength and higher ductility properties of the SM12 heats compared to previous 14YWT heats could be attributed to the lower O, C and N levels. Another point is that the different extrusion

(a)

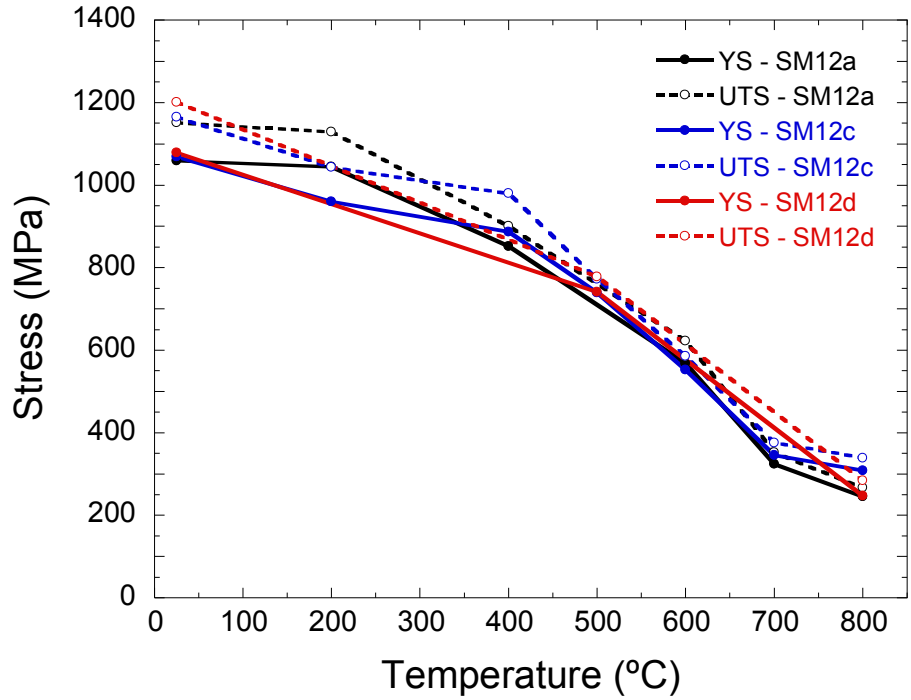

(b)

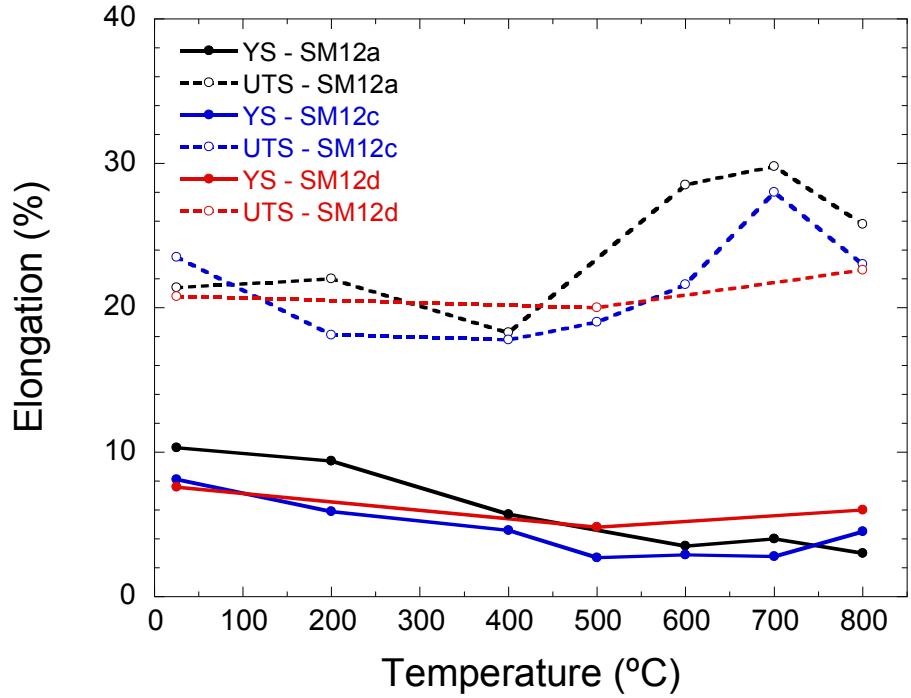

Figure 6. Results of the tensile tests conducted on specimens of the three 14YWT-SM12 heats over the temperature range from 25ºC to 800ºC. (a) Changes in yield and ultimate tensile stresses and (b) changes in uniform and total elongations as a function of temperatures.

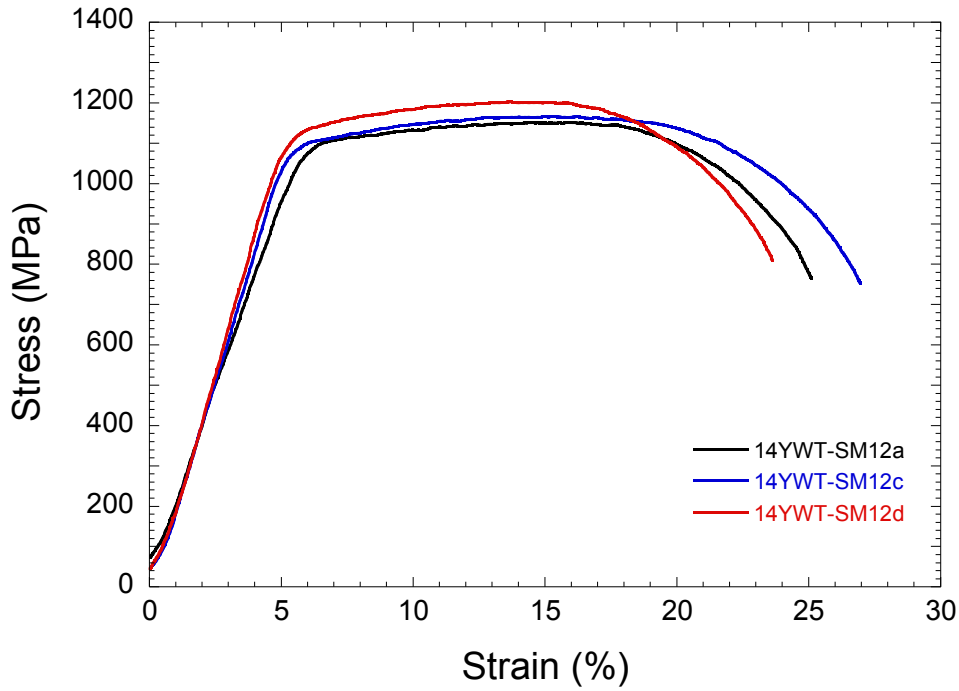

Figure 7. Comparison of stress strain curves from tensile tests at room temperature for the SM12a, SM12c and SM12d heats of 14YWT.

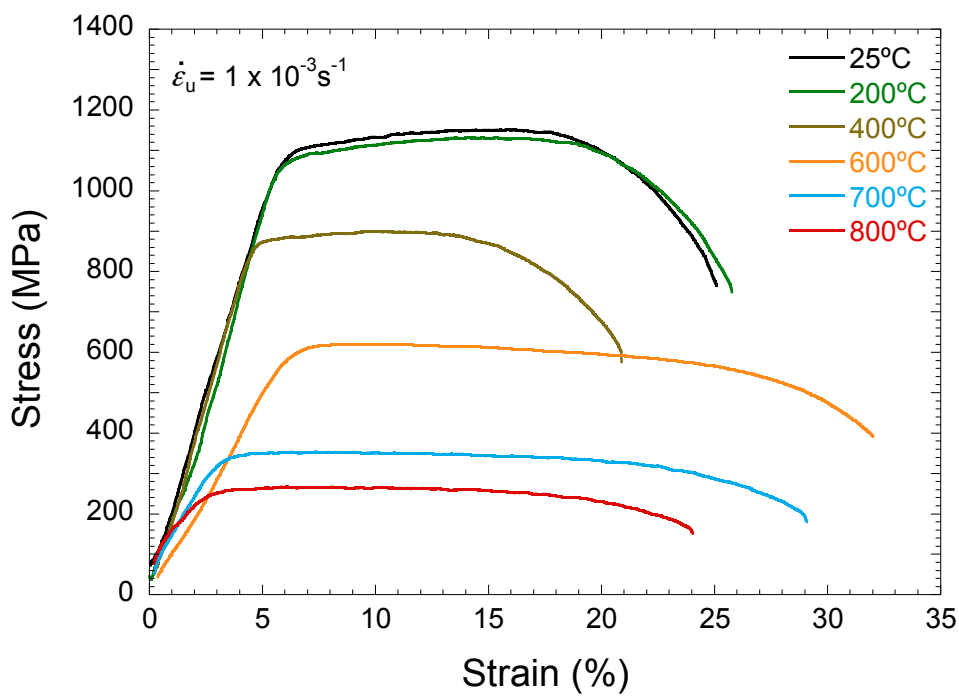

Figure 8. Stress strain curves from tensile tests ranging from 25ºC to 800ºC on 14YWT-SM12a.

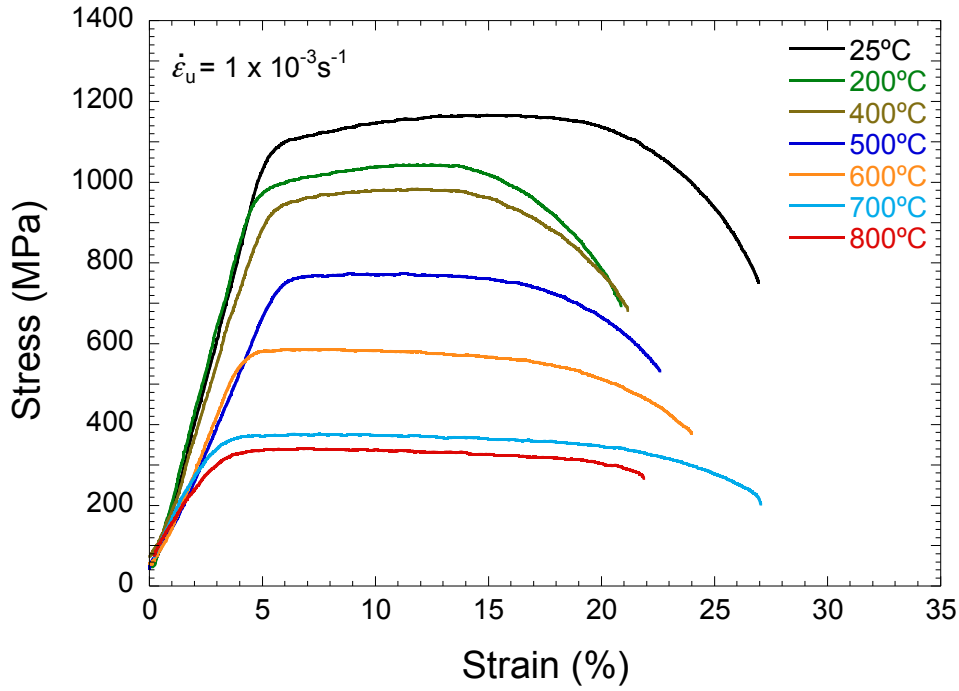

Figure 9. Stress strain curves from tensile tests ranging from 25ºC to 800ºC on 14YWT-SM12c.

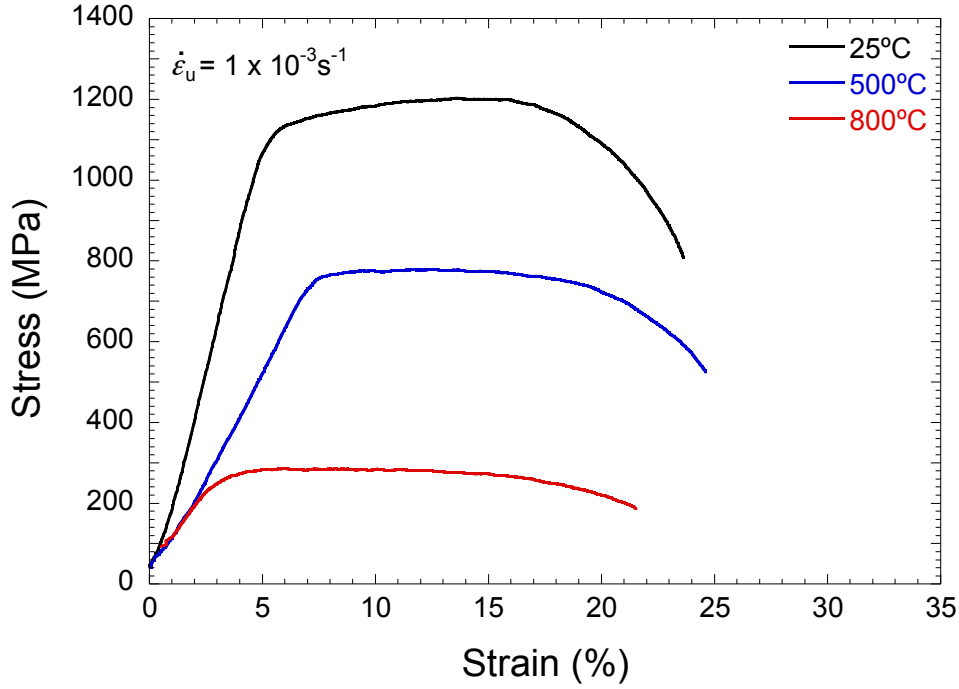

Figure 10. Stress strain curves from tensile tests ranging from 25ºC to 800ºC on 14YWT-SM12d.

temperatures had essentially no effect on the general microstructural features and tensile properties of the 14YWT-SM12 heats. The most likely reason for this result was due to the initial heat treatment that was performed on the cans containing the ball-milled powders used to produce the three heats. This heat treatment was for 1 h at 850ºC and was designed to form similar microstructures in the ball milled powders in each can before heat treating at the different temperatures for extruding the cans, which was for 1 h at 1150ºC for SM12a, 1000ºC for SM12c and 850ºC for SM12d. However, further microstructural characterization using advanced TEM techniques such as high angle annular dark field (HAADF) STEM imaging with the JEOL 2200FS-AC aberration-corrected STEM/TEM instrument and EFTEM analysis with the Philips CM200 TEM/STEM will be required to investigate more subtle differences in the nano-size oxide particle dispersions in the SM12 heats that will improve understanding the relationship between processing, mechanical properties and microstructure of the 14YWT-SM12 heats.

SUMMARY

Three heats of the advanced ODS 14YWT-SM12 ferritic alloy were produced by extrusion at different temperatures of 1150ºC (SM12a), 1000ºC (SM12c) and 850ºC (SM12d). Plate samples of the three heats were produced by rolling parallel to the extrusion direction at 1000ºC to 50% reduction in thickness. Results from tensile tests conducted over the temperature range from 25ºC to 800ºC showed lower strengths, but much better ductility in all the 14YWT-SM12 heats compared to results from previous 14YWT heats. The yield stresses and ultimate tensile strengths of the SM12 heats were ~1050 MPa and ~1200 MPa, respectively, at room temperature and decreased with temperature to ~260 MPa and ~300 MPa, respectively, at 800ºC. The uniform and total elongations of the SM12 heats were ~9-10% and ~21-24%, respectively, at room temperature. The TEM analysis of the 14YWT-SM12 heats showed that all three heats contained grains that were similar in size, size distribution and morphology. The microstructures consisted of grains that were mostly less than 1 mm in size with wide size distributions and slight elongated in the extrusion and rolling directions. The TEM results showed that the microstructures consisted of grains containing a low number density of particles larger than ~10 nm that were non-uniformly distributed. Both BF diffraction contrast imaging of the SM12 heats and initial EFTEM analysis of the SM12a heat revealed the presence of a high density of very small particles that were ~4-6 nm in size that were most likely the Ti-, Y- and O-enriched nanoclusters. However, this inference will need to be confirmed with additional EFTEM and atom probe analyses in the future.

FUTURE WORK

Detailed characterization of the microstructures and mechanical properties of the 14YWT-SM12 heats will continue. Since the ferromagnetic nature of the 3 mm dia. TEM disks prepared from the 14YWT-SM12 heats caused significant problems with alignment of the CM200 TEM/STEM, a set of new specimens will be prepared by lift-out of a small specimen (~10 mm x 8 mm x <1 mm thickness) from the polished section of the TEM disks and thinning by the Focused Ion Beam (FIB) method. These specimens will result in the achievement of better resolution with TEM imaging techniques. Several tensile tests will be conducted on specimens of the SM12a and SM12d heats to complete the high temperature tests. Fracture toughness (DCT) specimens were fabricated from the three heats and testing will focus on determining the fracture toughness transition temperature and possibly the fracture toughness at elevated temperatures.

ACKNOWLEDGEMENT

Research at Oak Ridge National Laboratory (ORNL) was sponsored by the Office of Fusion Energy Sciences, Office of Nuclear Energy, Science and Technology and research at the ORNL ShaRE Facility was supported in part by the Division of Scientific User Facilities, Office of Basic Energy Sciences, U.S. Department of Energy. ORNL is managed by UT-Battelle, LLC for the U.S. Department of Energy.

REFERENCE

1. D. T. Hoelzer, E. T. Manneschmidt, and M. A. Sokolov, Fusion Materials Semiannual Progress Report for the Period Ending December 31, 2011, DOE/ER-0313/51, Vol. 51, 2011, P. 22-31.
2. J. Bentley, D. T. Hoelzer, D. W. Coffey and K. A. Yarborough, *Microsc. Microanal.* **10**, Issue S02 (2004) 662-663.